Electronic band gap of van der Waals α-As2Te3 crystals

Lama Khalil, Jean-Christophe Girard, Debora Pierucci, Federico Bisti, Julien Chaste, Fabrice Oehler, Charlie Gréboval, Ulrich Nguétchuissi Noumbé, Jean-Francois Dayen, Demetrio Logoteta, et al.

Electronic band gap of van der Waals α-As_2Te_3 crystals

Lama Khalil[1], Jean-Christophe Girard[1], Debora Pierucci[1], Federico Bisti[2], Julien Chaste[1], Fabrice Oehler[1], Charlie Gréboval[3], Ulrich Nguétchuissi Noumbé[4], Jean-Francois Dayen[4,5], Demetrio Logoteta[1], Gilles Patriarche[1], Julien Rault[6], Marco Pala[1], Emmanuel Lhuillier[3], & Abdelkarim Ouerghi*[1]

[1]Université Paris-Saclay, CNRS, Centre de Nanosciences et de Nanotechnologies, 91120, Palaiseau, France
[2]CELLS - ALBA Synchrotron Radiation Facility, Carrer de la Llum 2-26, 08290 Cerdanyola del Valles, Barcelona, Spain
[3]Sorbonne Université, CNRS, Institut des NanoSciences de Paris, INSP, F-75005 Paris, France
[4]Université de Strasbourg, IPCMS-CMRS UMR 7504, 23 Rue du Loess, 67034 Strasbourg, France
[5]Institut Universitaire de France, 1 rue Descartes, 75231 Paris cedex 05
[6]Synchrotron-SOLEIL, Saint-Aubin, BP48, F91192 Gif sur Yvette Cedex, France

Corresponding Author: abdelkarim.ouerghi@c2n.upsaclay.fr

van der Waals materials offer a large variety of electronic properties depending on chemical composition, number of layers, and stacking order. Among them, As_2Te_3 has attracted attention due to the promise of outstanding electronic properties, and high photo-response. Precise experimental determinations of the electronic properties of As_2Te_3 are yet sorely needed for better understanding of potential properties and device applications. Here, we study the structural and electronic properties of α-As_2Te_3. Scanning transmission electron microscopy coupled to energy X-ray dispersion (STEM-EDX), and micro-Raman spectroscopy all confirm that our specimens correspond to α-As_2Te_3. Scanning tunneling spectroscopy (STS) at 4.2K demonstrates that α-As_2Te_3 exhibits an electronic band gap of about 0.4 eV. The material can be exfoliated, revealing the (100) anisotropic surface. Transport measurements on a thick exfoliated sample (bulk-like) confirm the STS results. These findings allows for a deeper understanding of the As_2Te_3 electronic properties, underlying the potential of V-VI semiconductors for electronic and photonic technologies.

Keywords: As_2Te_3, Electronic Band Gap, Electronic Transport, Field Effect Transistor

Following the successful isolation of monolayer (ML) graphene, many other two-dimensional (2D) van der Waals lamellar (vdW) compounds have been investigated. “Honeycombs hexagonal” ML materials, such as transition metal dichalcogenides (TMDs)[1,2,3], metal mono-chalcogenides (GaSe, InSe, GaTe)[4–8] and Xenes (X = Si, Ge, Sn, P, As, Sb, Bi, Te)[9] have attracted considerable attention from both physics and chemistry communities. Similarly, “buckled” ML from monoelemental group-V and –VI compounds (phosphorene, arsenene, tellurium, antimonene and bismuthene) are particularly interesting, due to high stretchability of the buckled structure[9] and the related strain modification on their band. Beyond these well-known examples, other materials crystallize in a vdW lamellar stacking, with slightly more complex ML crystal structure. The α-As_2Te_3 shows a “buckled”-like ML structure, and display a rather unique combination of properties, which are of interest for fundamental studies of anisotropic phenomena in 2D materials, but could also enable new types of applications such as acousto-optic modulators.

Despite the general interest in layered semiconductors, many optical and electronic properties of crystalline As_2Te_3 are unknown[10]. As_2Te_3 exist in two different crystal structures, α- and β-, originating from distinct stacking sequences, which share the same composition. This polymorphism likely affects the electronic and physical properties of As_2Te_3. Yet, there is no report on the band structure properties of crystalline phases of α and β-As_2Te_3 even at room conditions. The α-As_2Te_3 phase display a monoclinic structure[11] which is composed of repeats of staircase pattern (4 As atoms sandwiched by 6 Te atoms) (Figure 1a)). Along the crystal axis a, these staircase units are simply stacked by van der Waals (vdw) interactions, creating an easy cleavage (100) plane. Inside each ML, the structure is very asymmetric with regular infinite chains along b and weak covalent bounding between staircase units along c. The α-As_2Te_3 ML thus displays a strong in plane anisotropy and 1D-like behavior. Several preceding investigations have focused on the phase transition induced in α-As_2Te_3[12], but no one has determined experimentally any basic electronic parameters, such as the electronic band gap.

We report here a STM/STS and transport study of the electronic properties of monolayer As_2Te_3. This study was also supported by micro-Raman spectroscopy and STEM for morphological and elemental assessments. The STM images demonstrate a large atomically ordered flat region with ligne defect. The Fourier transform indicates a spatial periodicity of 4.0 Å and 9.9 Å in perpendicular directions, which is consistent with the lattice parameters the monoclinic structure determined by Raman spectroscopy and STEM. This confirms that the exposed cleaved surface is the (100), as expected from the weak vdW stacking along the [100] direction.

Our sample is a commercial α-As_2Te_3 crystal from HQ Graphene (http://www.hqgraphene.com/). To determine the crystal structure of our As_2Te_3 samples, we conducted a comprehensive characterization by employing complementary techniques. The µ-Raman measurements were conducted using a commercial confocal HORIBA LabRAM HR operating at 532 nm[13]. The incident photon beam was focused down to a submicrometric spot (~1 µm in diameter) on the sample. Concerning the vibrational properties of α-As_2Te_3, 30 zone-center phonons belong to the $\Gamma = 10(A_g + B_u) + 5(A_u + B_g)$ mechanical representation at the center of the BZ. Among these phonon modes, the gerade (g) modes are Raman active, while the ungerade (u) modes are infrared active, excluding 1 A_u and 2 B_u modes, which are acoustic modes[14]. Thus, α-As_2Te_3 has in total 15 phonon modes that are Raman active. Note that the A_u and B_g modes involve atomic displacements along the *b* axis, whereas the A_g and B_u modes are relative to

vibrations in the a-c atomic plane. Figure 1(b) displays the typical μ-Raman scattering spectrum of our samples in the frequency range of 22-215 cm^{-1}. The μ-Raman spectra show 10 out of the 15 Raman active mode peaks, together with the position of the center of the fitting components, indicated with red markers; the fitting was performed using a Voigt function. In particular, we notice peaks at 43.1 cm^{-1}, 48 cm^{-1}, 64 cm^{-1}, 67.3 cm^{-1}, 88.9 cm^{-1}, 97.4 cm^{-1}, 120.6 cm^{-1}, 137.4 cm^{-1}, 171.5 cm^{-1} and 193.1 cm^{-1}, corresponding to the A_g^1, A_g^2, B_g^2, A_g^3, A_g^4, B_g^3, A_g^6, B_g^5, A_g^8 and A_g^{10} modes, respectively. The assignment of these phonon modes was carried out in accordance with the work performed by Cuenca-Gotor *et al.*[14], and is coherent with the α-phase of As_2Te_3.

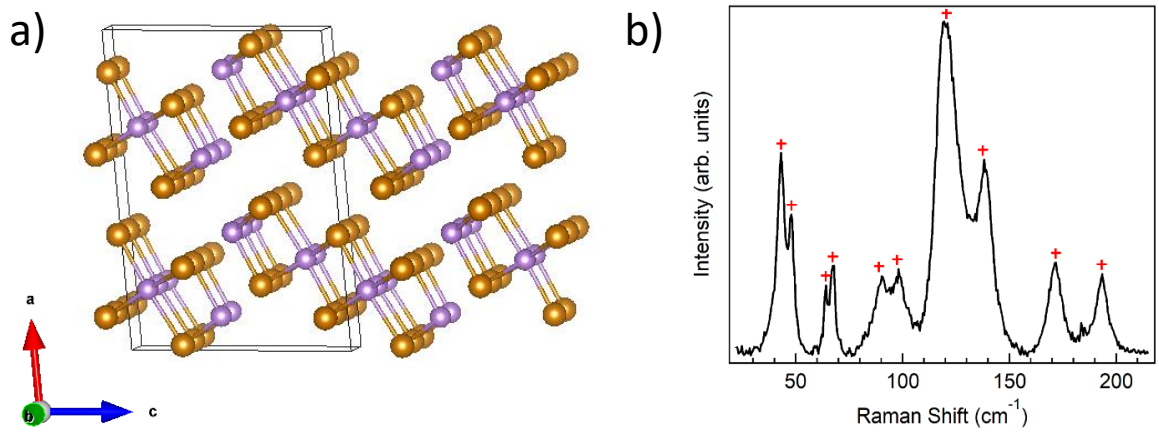

Figure 1: Crystallographic and μ-Raman analysis of α-As_2Te_3: a) Crystal structure of α-As_2Te_3. Arsenic and tellurium atoms are represented in purple and orange spheres, respectively, b) μ-Raman spectrum acquired at room temperature from the α-As_2Te_3 crystal, showing 10 Raman peaks. The red markers refer to the center of the fitting components.

Figure 2 shows a transmission electron microscopy (TEM, FEI Titan Themis operating at 200 kV) analysis of a cleaved bulk As_2Te_3 crystal. By mechanical cleaving, we were able to obtain a thin enough sample so that standard scanning TEM (STEM) coupled to chemical analysis, using energy dispersive X-ray spectroscopy (EDX, Brucker super X), could be performed. A large view of the probed area is shown Fig. 2a, acquired in the STEM mode using the high angle annular dark field detector (HAADF). The complementary EDX analysis reveals that the sample is homogeneously composed of As (Fig. 2b) and Te (Fig. 2c). EDX quantification indicates an atomic ratio of 2:3, as expected from the As_2Te_3 stoichiometry. Standard HR-TEM shows fringes at the edge of the sample (Fig. 2d), which indicates that the material is crystalline. Further analysis by HR-STEM (Fig. 2f) is obtained by zooming in the probed region (Fig. 2d, white rectangle). The corresponding Fourier transform (FFT) is shown Figs. 2e. Indexation of the various reflections using length and angle match those of monoclinic α-As_2Te_3 (a = 14.345 Å, b = 4.016 Å, c = 9.891 Å and β = 95.06°) and determine the zone axis as [011]. Using this information, we combine in Fig. 2f the atomic resolution HR-STEM (HAADF) image of the sample in real space with the expected crystal structure of α-As_2Te_3, viewed along the [011] zone axis. In this particular projection, the atomic columns are exclusively composed of As or Te atoms. Consequently, Te columns (Z = 52) appear much brighter than As columns (Z = 33) in this HAADF image, due to the large Z contrast difference. The qualitative contrast and the location of each atomic column in the STEM image match those of the α-As_2Te_3 crystal structure. In conclusion,

the chemical and structural analysis of the region probed by TEM unambiguously determines the material as homogeneous monoclinic α-As_2Te_3.

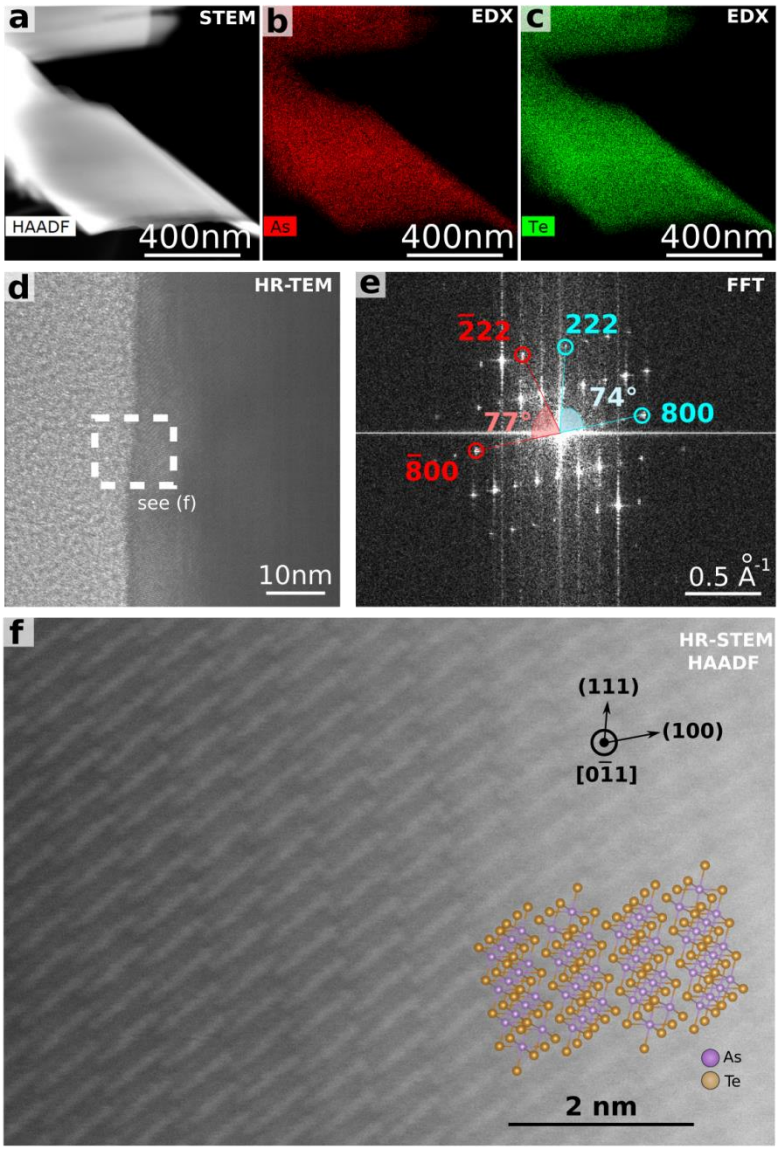

Figure 2: TEM analysis of α-As_2Te_3: a-c Large scale view (STEM) (**a**) and its corresponding chemical maps (EDX) (**b**, **c**) of the material, showing the homogeneous elemental distributions of As and Te. **d** Conventional HR-TEM showing the crystalline nature of the sample and the zone selected (white rectangle) for further analysis by HR-STEM. **e** Fourier transform of the HR-STEM image shown in (**f**) presenting the reciprocal lattice and the theoretical reflections of α-As_2Te_3. **f** Atomically resolved HR-STEM image, superposed with the crystal structure of α-As_2Te_3, viewed along the [011] zone axis.

Having established the phase structure of α-As_2Te_3, we now discuss its electronic properties by means scanning tunneling microscopy/spectroscopy (STM/STS) taken at 4.2 K. For these STM/STS measurements, the crystal was prepared by *in situ* cleaving in UHV[8]. Due to the weak vdW stacking along the crystal axis a, we expect a (100) cleavage plane. Figure 3(a) shows a large-scale topographic STM image the UHV-cleaved surface of α-As_2Te_3, revealing the presence of a high density of step edges and line defects on this surface. In the corresponding zoomed-in STM image to Fig. 3(b), we notice the presence of large atomically ordered flat regions, reflecting the high

quality of our sample. The surface electronic structure clearly displays a rectangular symmetry, which is confirmed by the corresponding Fourier transform (see inset of Fig. 3(b)). We measure a spatial periodicity of 4.0 Å and 9.9 Å in perpendicular directions, which is consistent with the lattice parameters *b* and *c* of the monoclinic structure previously determined by Raman spectroscopy and STEM (Fig. 1 and 2). This confirms that the exposed surface is (100), as expected from the lamellar vdW crystal structure.

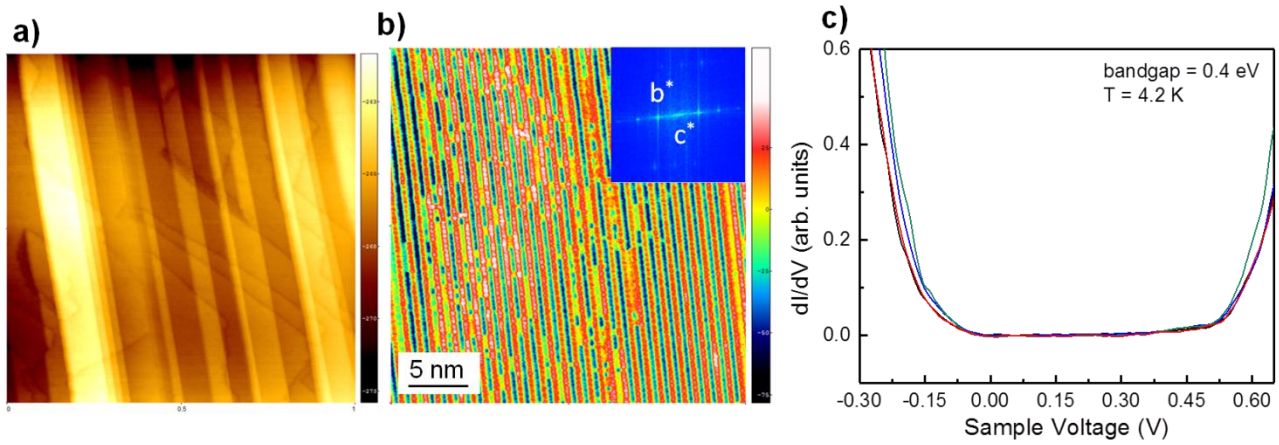

Fig. 3: Crystallographic and electronic properties of α-As_2Te_3: a) Large-scale STM image of the UHV-cleaved surface of α-As_2Te_3 (1000 x 1000 nm^2), revealing the high density of step edges and line defects on this surface. b**)** Corresponding zoomed-in STM image to Fig. 1e (30 x 30 nm^2) (V_{bias} = -0.7 eV, $I_{tunneling}$ = 100 pA and T = 4.2 K). Inset: Fourier transform of the topographic image, confirming the (100) surface orientation, **c)** The differential conductance (dI/dV) spectrum as a function of the bias voltage showing that the energy bandgap is of 0.4 eV.

Then, we probed the electronic structure of α-As_2Te_3 by means of STS. A typical spectrum of the differential conductance (dI/dV) measured as a function of the bias voltage is shown in Fig. 3(c). The I(V) characteristics were acquired while the feedback loop was inactive, and the differential conductivity *dI/dV* was measured directly by using the lock-in technique. The differential conductance (*dI/dV*) is proportional to the local occupied and unoccupied density of states below and above E_F, As the edges of the valence and conduction bands are observed to be around -0.032 eV and 0.368 eV, respectively, the electronic quasiparticle bulk bandgap is hence of 0.4 eV. The Fermi energy, corresponding to the zero bias in the *dI/dV* spectrum, is positioned slightly below the mid-gap value, suggesting the presence of a small concentration of intrinsic charged defects in our specimens and slight p-type doping.

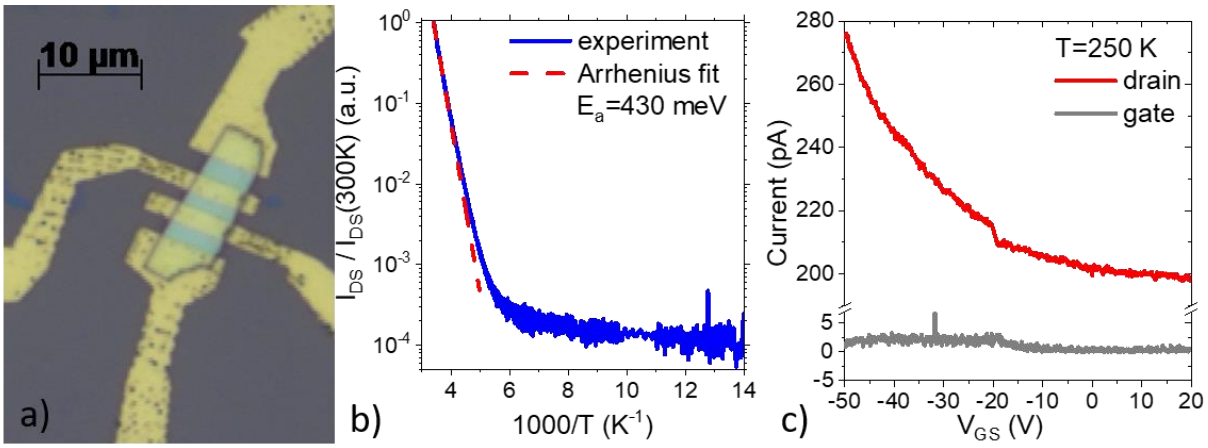

Figure 4: a) Optical microscopy image of an exfoliated As_2Te_3 flake connected to Ti/Au electrodes, b) Current of the sample under 0.25 V, normalized by its value at room temperature, as a function of the temperature. An Arrhenius fit is also show presenting an activation energy of 430 meV, c) Transfer curve (drain and gate current as a function of gate bias under constant drain source bias set equal to 0.5 V) for a field effect transistor which channel is made of the As_2Te_3 flake. All measurements are performed at 250 K.

Finally, we have studied electronic transport in our α-As_2Te_3 sample. To this end, a bulk As_2Te_3 crystal was mechanically exfoliated using adhesive tapes, and then transferred onto Si/SiO_2 substrate (400 nm of oxide), before being connected to Ti/Au electrodes fabricated by e-beam lithography (see Fig. 4a and supplementary information). Atomic force microscopy (supplementary information Fig S1) reveals a thickness of 150 nm for the exfoliated material, meaning that sample has bulk-like properties. We then measure the transport properties[15]. Fig. 4b shows the temperature-dependence of the sample conductance (see also additional measurement, supplementary information Fig S2). In the range of temperature between 300 K and 150 K, we observe a fast drop of the conductance as the temperature increases, which can be fitted by an Arrhenius law with an activation energy around 430 meV. In this range of temperature (250 K), field effect transistor measurements reveal that residual conduction is due to holes (i.e., increase of the conductance under negative bias), as shown in Fig. 4c. Below 150 K, the sample becomes highly insulating and R stabilizes to a value below ≈ 10^{12} Ω. Illumination of the sample by a laser diode at 1.55 µm (0.8 eV), shows a clear increase of the current (supplementary information Fig S3) which confirms the presence of a narrower band gap in this system. The transport measurements correlate extremely well with the STS data and confirm a semi-conductor behavior with a energy gap of about 0.4 eV, with p-type conductivity in the probed temperature range.

In summary, we report an experimental study of electronic and transport properties of α-As_2Te_3. The material can be exfoliated along the weak [100] direction, exposing the asymmetric (100) surface. The latter is strongly anisotropic, with a buckled pattern (c direction) assembled in long parallel chains (b direction). Scanning tunneling spectroscopy and electronic transport measurements show that bulk α-As_2Te_3 is a semiconductor with a band gap about 0.4 eV, with potential applications in electronics or opto-electronics.

Acknowledgments

We acknowledge Hervé Cruguel for conducting AFM measurements. We acknowledge the financial support by RhomboG (ANR-17-CE24-0030), MagicValley (ANR-18-CE24-0007) and Graskop (ANR-19-CE09-0026) grants. We also thank the support ERC starting grant blackQD (grant n° 756225). This work is supported by a public grant overseen by the French National Research Agency (ANR) as part of the "Investissements d'Avenir" program (Labex NanoSaclay, ANR-10-LABX-0035).

References :

(1) Liu, K. K.; Zhang, W.; Lee, Y. H.; Lin, Y. C.; Chang, M. T.; Su, C. Y.; Chang, C. S.; Li, H.; Shi, Y.; Zhang, H.; *et al.* Growth of Large-Area and Highly Crystalline MoS 2 Thin Layers on Insulating Substrates. *Nano Lett.* **2012**, *12*, 1538–1544.

(2) Ambrosi, A.; Sofer, Z.; Pumera, M. 2H → 1T Phase Transition and Hydrogen Evolution Activity of MoS2 , MoSe2 , WS2 and WSe2 Strongly Depends on the MX2 Composition. *Chem. Commun.* **2015**, *51*, 8450–8453.

(3) Chang, C. H.; Fan, X.; Lin, S. H.; Kuo, J. L. Orbital Analysis of Electronic Structure and Phonon Dispersion in MoS 2, MoSe2, WS2, and WSe2 Monolayers under Strain. *Phys. Rev. B - Condens. Matter Mater. Phys.* **2013**, *88*, 1–9.

(4) Cao, T.; Li, Z.; Louie, S. G. Tunable Magnetism and Half-Metallicity in Hole-Doped Monolayer GaSe. *Phys. Rev. Lett.* **2015**, *114*, 236602.

(5) Ben Aziza, Z.; Henck, H.; Pierucci, D.; Silly, M. G.; Lhuillier, E.; Patriarche, G.; Sirotti, F.; Eddrief, M.; Ouerghi, A. Van Der Waals Epitaxy of GaSe/Graphene Heterostructure: Electronic and Interfacial Properties. *ACS Nano* **2016**, *10*, 9679–9686.

(6) Si, C.; Lin, Z.; Zhou, J.; Sun, Z. Controllable Schottky Barrier in GaSe/Graphene Heterostructure: The Role of Interface Dipole. *2D Mater.* **2016**, *4*, 015027.

(7) Balakrishnan, N.; Steer, E. D.; Smith, E. F.; Kudrynskyi, Z. R.; Kovalyuk, Z. D.; Eaves, L.; Patanè, A.; Beton, P. H. Epitaxial Growth of γ-InSe and α, β, and γ-In2Se3on ϵ-GaSe. *2D Mater.* **2018**, *5*.

(8) Aziza, Z. B.; Pierucci, D.; Henck, H.; Silly, M. G.; David, C.; Yoon, M.; Sirotti, F.; Xiao, K.; Eddrief, M.; Girard, J.-C.; *et al.* Tunable Quasiparticle Band Gap in Few Layer GaSe/Graphene Van Der Waals Heterostructures. *arXiv*, 2017.

(9) Lei, W.; Portehault, D.; Dimova, R.; Antonietti, M. Boron Carbon Nitride Nanostructures from Salt Melts: Tunable Water-Soluble Phosphors. *J. Am. Chem. Soc.* **2011**, *133*, 7121–7127.

(10) Morin, C.; Corallini, S.; Carreaud, J.; Vaney, J.-B.; Delaizir, G.; Crivello, J.-C.; Lopes, E. B.; Piarristeguy, A.; Monnier, J.; Candolfi, C.; *et al.* Polymorphism in Thermoelectric As2Te3. *Inorg. Chem.* **2015**, *54*, 9936–9947.

(11) Carron, G. J. The Crystal Structure and Powder Data for Arsenic Telluride. *Acta Crystallogr.* **1963**, *16*, 338–343.

(12) Morin, C.; Corallini, S.; Carreaud, J.; Vaney, J. B.; Delaizir, G.; Crivello, J. C.; Lopes, E. B.; Piarristeguy, A.; Monnier, J.; Candolfi, C.; *et al.* Polymorphism in Thermoelectric As2Te3. *Inorg. Chem.* **2015**, *54*, 9936–9947.

(13) Zribi, J.; Khalil, L.; Zheng, B.; Avila, J.; Pierucci, D.; Brulé, T.; Chaste, J.; Lhuillier, E.; Asensio, M. C.;

Pan, A.; *et al.* Strong Interlayer Hybridization in the Aligned SnS<inf>2</Inf>/WSe<inf>2</Inf> Hetero-Bilayer Structure. *npj 2D Mater. Appl.* **2019**, *3*.

(14) Cuenca-Gotor, V. P.; Sans, J. A.; Ibáñez, J.; Popescu, C.; Gomis, O.; Vilaplana, R.; Manjón, F. J.; Leonardo, A.; Sagasta, E.; Suárez-Alcubilla, A.; *et al.* Structural, Vibrational, and Electronic Study of α-As2Te3 under Compression. *J. Phys. Chem. C* **2016**, *120*, 19340–19352.

(15) Henck, H.; Pierucci, D.; Chaste, J.; Naylor, C. H.; Avila, J.; Balan, A.; Silly, M. G.; Asensio, M. C.; Sirotti, F.; Johnson, A. T. C.; *et al.* Electrolytic Phototransistor Based on Graphene-MoS2 van Der Waals p-n Heterojunction with Tunable Photoresponse. *Appl. Phys. Lett.* **2016**, *109*, 113103.